Technical report on the design of extension springs for the 2-RRS-1-RRRR mechanism

Isaac John[1], Santhakumar Mohan[1], and Philippe Wenger[2]

[1]Department of Mechanical Engineering, Indian Institute of Technology Palakkad 678623, Kerala, India
[2]Ecole Centrale de Nantes, CNRS, LS2N, Nantes Universite, Nantes 44000, France

1 Introduction

This report investigates two strategies for the design of extension springs suitable for various proportions of a two-degrees-of-freedom (dof), 2-RRS-1-RRRR cable-actuated mechanism.

The 2-RRS-1-RRRR mechanism, depicted in Fig. 1, has a moving platform connected to a fixed base by an R⊥R‖R⊥R (R-revolute joint) limb and two R⊥RS (S-spherical joint) limbs. The proximal R joints of the three limbs are attached to the base at radial coordinates $(r,\ \beta_i)$, $\beta_i = 90°,\ 210°,\ 330°$, for $i = 1, 2, 3$, with respect to the X_B axis of the base frame. The distal R joint of the RRRR limb and the S joints of the RRS limbs are attached to the moving platform at radial coordinates $(r,\ \gamma_i)$, $\gamma_i = 270°,\ 30°,\ 150°$, for $i = 1, 2, 3$, with respect to the X_P axis of the platform frame.

The mechanism is actuated by three cables with mounting points on the base and moving platforms having radial coordinates (r', β_i), where $\beta_i = 90°,\ 210°,\ 330°$, with respect to the X_B axis (for the base) and the X_P axis (for the moving platform). Three springs are attached in parallel to the actuation cables to prevent the mechanism from collapsing in an inactive state with zero actuation forces, and to contribute to the overall stiffness of the mechanism.

The pose of the platform is defined using three position coordinates $p_x,\ p_y,\ p_z$ and three X(θ)-Y(ψ)-Z(ϕ) Euler angles. For inverse kinematics,

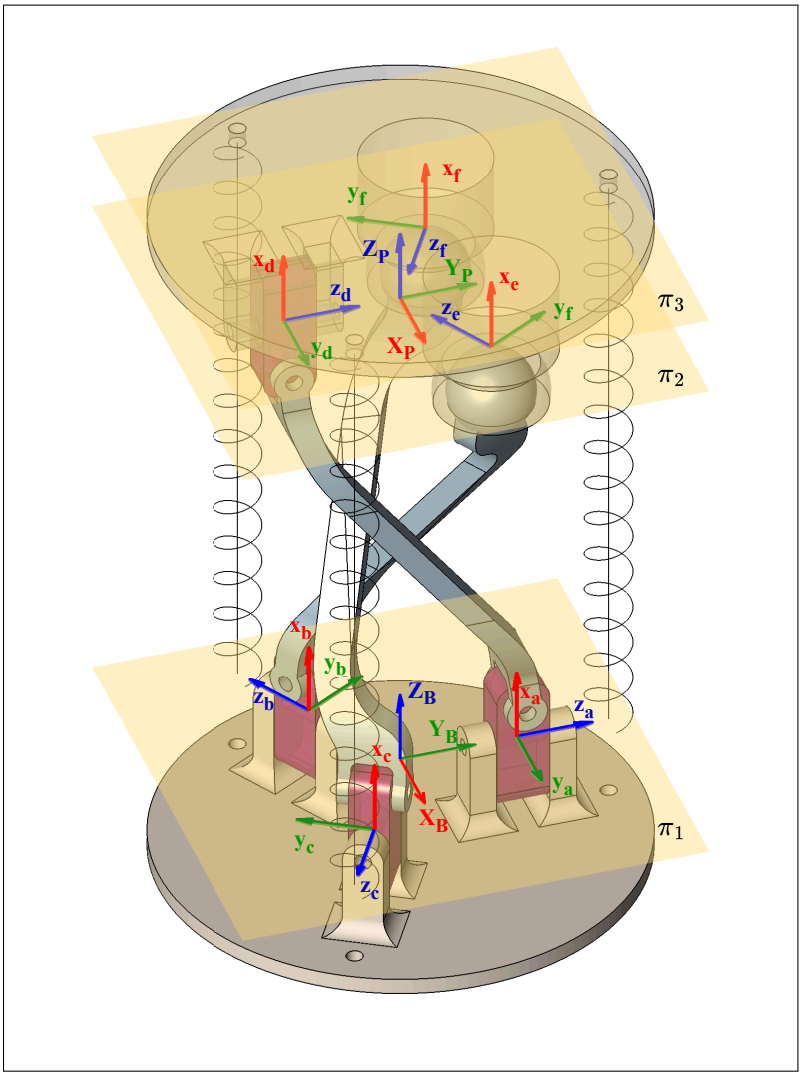

Figure 1: The 3-cable-actuated 2-dof 2-RRS-1-RRRR parallel mechanism. Three limb local frames $\{a\}$, $\{b\}$, and $\{c\}$ are attached at the proximal ends of the three limbs. The z_i axis, $i = a, b, c$, is aligned along the first R axis at the proximal end, and the x_i axis is perpendicular to the plane of the base platform. Similarly, three frames $\{d\}$, $\{e\}$, and $\{f\}$ are attached at the distal ends of the three limbs. The proximal frames $\{a\}$, $\{b\}$, and $\{c\}$, and the base frame $\{B\}$ lie on the plane π_1. The distal frames $\{d\}$, $\{e\}$, and $\{f\}$, and the moving platform frame $\{P\}$ lie on the plane π_2. The plane π_3 is offset from π_2 and lies on the nearest circular face of the moving platform. The springs and cables are mounted on the π_1 plane at their proximal ends and on the π_3 plane at their distal ends.

the two Euler angles θ and ψ are considered as independent input parameters, while the remaining four (dependent) task-space variables ϕ, p_x, p_y, p_z are solved using the loop-closure constraints [1].

In our earlier works, the effects of the cable actuation forces and the link proportions on the mechanism's stiffness modulation capabilities were investigated. Until now, we have only considered zero-free-length springs with specific spring constants. We have continued with this assumption even while investigating the kinetostatics of the 2-RRS-1-RRRR cable-actuated mechanism of various proportions [2]. However, in all practical situations, an extension spring has a finite free length and requires a preload to elongate. The maximum extension is limited by the stresses developed, which have been neglected thus far.

The design strategies investigated in this report seek feasible designs for extension springs conforming to geometrical constraints on free length and outer coil diameter, as well as strength-based constraints defined by factors of safety at critical locations in the coil and hooks.

2 Design strategy 1: Only the free length and the maximum extended length are considered as inputs

The objective of this study is to obtain feasible extension spring designs that can be adopted for a 2-RRS-1-RRRR cable-actuated mechanism with a workspace range $(\theta, \psi) \in [-40°,\ 40°]$. The free length and the length at maximum extension shall be determined based on the range of link dimensions considered for the 2-RRS-1-RRRR mechanism.

2.1 Range of link dimensions for the 2-RRS-1-RRRR mechanism

The lower limit (resp. upper limit) of link lengths of the mechanism with stockier (resp. slender) proportions is provided in Table 1.

Proportions	l (mm)	h_1 (mm)	h_2 (mm)	r (mm)	r' (mm)
Stockier	150	0	0	45	72.5
Slender	150	10	10	35	62.5

Table 1: Range of link dimensions of the 2-RRS-1-RRRR mechanism for which an extension spring must be designed.

The free length of the extension spring should be less than the minimum distance between the attachment points of the springs at the top and bottom platforms of the mechanism in its stockiest proportion. The attachment points of the three springs at the base (resp. top) platforms are at radial coordinates $(r', 90°)$, $(r', 210°)$, and $(r', 330°)$ with respect to the base frame $\{B\}$ (resp. top platform frame $\{P\}$).

By studying various configurations of the mechanism evaluated on a square grid of $\theta \in [-40°,\ 40°]$ and $\psi \in [-40°,\ 40°]$, it was inferred that the **minimum distance = 80.62 mm** occurs at location 2 $(r', 210°)$ when $\theta, \psi = 40°,\ -40°$ and at location 3 $(r', 330°)$ when $\theta, \psi = 40°,\ 40°$.

For safe operating conditions, the maximum extension length of the spring should be greater than the maximum distance between the attachment points of the springs at the top and bottom platforms of the mechanism in its slenderest proportions. Once again, by studying various configurations of the mechanism with slender proportions on a square grid of $\theta \in [-40°,\ 40°]$ and $\psi \in [-40°,\ 40°]$, it was inferred that the **maximum distance = 232.19 mm** occurs at location 2 $(r', 210°)$ when $\theta, \psi = -40°,\ 40°$ and at location 3 $(r', 330°)$ when $\theta, \psi = -40°,\ -40°$.

Thus, a spring design with a free length $L_0 = 75$ ***mm and a maximum extended length*** $L_{max} = 235$ ***mm shall be developed.*** We follow the design practices of mechanical springs in [3].

2.2 Stress acting in the body of the extension spring

The maximum shear stress acting on the spring's coils is determined by the superposition of the direct shear stress $\tau_{direct} = \frac{4F}{\pi d^2}$ and the torsional shear stress $\tau_{torsion} = \frac{16FD}{\pi d^3}$, expressed mathematically as:

$$\tau_{coil} = \frac{4F}{\pi d^2} + \frac{16FD}{\pi d^3} \tag{1}$$

where d is the wire diameter and D is the mean coil diameter. Equation 1 is only valid when the curvature of the wire is not accounted for. If the curvature of the coil is also taken into consideration, a higher value of coil stress is expected, which is expressed by the following equation [3]:

$$\tau_{coil} = K_B \frac{8FD}{\pi d^3}, \quad K_B = \frac{4C+2}{4C-3}, \quad C = \frac{D}{d} \tag{2}$$

where the factor K_B, called the Bergsträsser factor, accounts for the effect of curvature in estimating the stress, and C, called the spring index, is preferred to be in the range [4, 12].

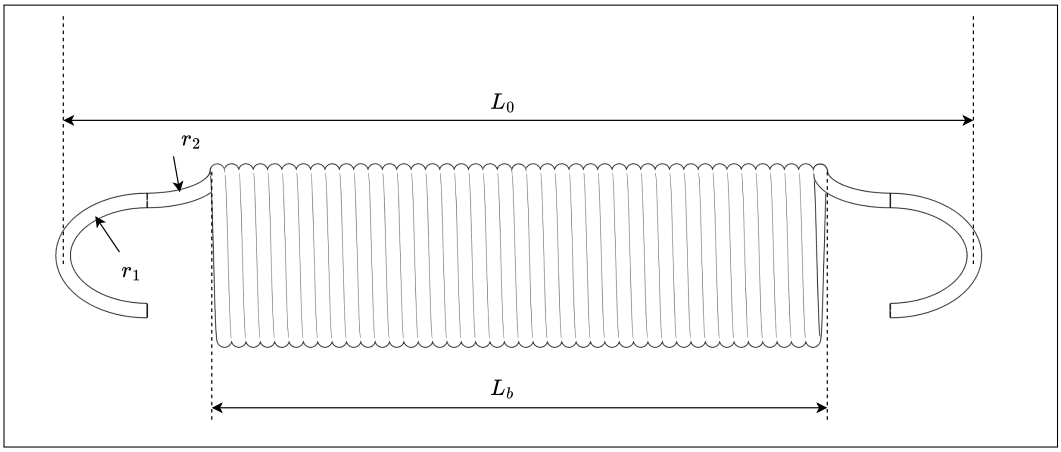

(a)

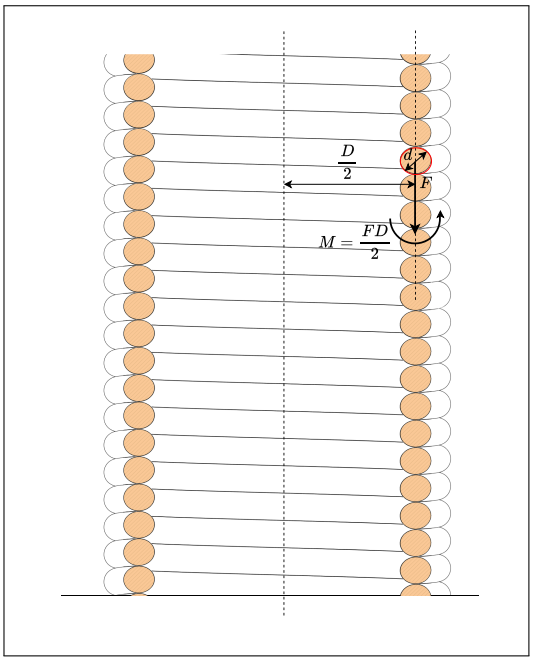

(b)

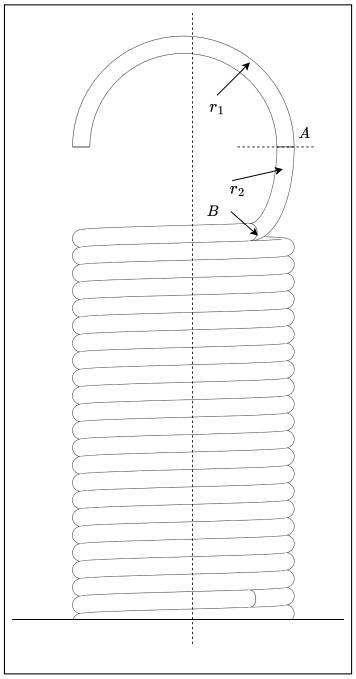

(c)

Figure 2: An extension spring with half-machined hooks on either side (2a). The shear stress acting on the coils is contributed by the tension F and the torque M due to transferring the tensile load F by a distance $D/2$ (2b). The maximum tensile stress occurs at point A on the hook due to tensile and bending forces, and the maximum shearing stress on the hook occurs at B due to the twisting effect of the axial tensile force F (2c).

2.3 Stresses acting on the hooks of the extension spring

The maximum tensile stress, contributed by the axial and bending loads, occurs at section A in Fig. 2c. The curvature-corrected tensile stress is expressed as:

$$\sigma_A = F\left[(K)_A \frac{16D}{\pi d^3} + \frac{4}{\pi d^2}\right], \quad (K)_A = \frac{4C_1^2 - C_1 - 1}{4C_1(C_1 - 1)}, \quad C_1 = \frac{2r_1}{d} \tag{3}$$

where $(K)_A$ is the curvature correction factor for bending stress. The maximum torsional stress occurs at section B, as shown in Fig. 2c [4]. The mathematical expression is:

$$\tau_B = (K)_B \frac{8FD}{\pi d^3}, \quad (K)_B = \frac{4C_2 - 1}{4C_2 - 4}, \quad C_2 = \frac{2r_2}{d} \tag{4}$$

where $(K)_B$ is the stress correction factor for curvature.

2.4 Material properties

We shall consider the spring material to be ASTM 228 music wire, whose material properties are presented in Table 2.

Material property	Value
Modulus of Elasticity E	203.4 GPa, $d < 0.032$ mm 200 GPa, $0.033 < d < 0.063$ mm 196.5 GPa, $0.064 < d < 0.125$ mm 193 GPa, $d > 0.125$ mm
Modulus of Rigidity G	82.7 GPa, $d < 0.032$ mm 81.7 GPa, $0.033 < d < 0.063$ mm 81 GPa, $0.064 < d < 0.125$ mm 80 GPa, $d > 0.125$ mm
Tensile ultimate strength S_{ut}	$\frac{2211}{d^{0.145}}$ MPa, $0.1 < d < 6.5$ mm
Tensile yield strength S_y	$0.75S_{ut}$ MPa
Torsional yield strength S_{sy}	$0.45S_{ut}$ MPa

Table 2: Material properties of ASTM 228 music wire.

2.5 Problem statement

It is required to design a spring with:

- Free length $L_0 = 75$ mm.

- Maximum extended length $L_{max} = L_0 + y_{max} = 235$ mm, where y_{max} is the maximum elongation from the free length.
- The outer diameter OD $(= d + D)$ is fixed at 15 mm for practical considerations.
- The hook radius shall be constrained as $r_1 = 0.5D$ and may be changed if the tensile stress σ_A exceeds permissible limits.
- The feasible designs should be such that the spring index $C = D/d$ lies in the interval [4, 12].
- Furthermore, the following constraint is to be enforced:

$$L_0 = L_b + 2(r_1 + r_2), \quad \text{where} \quad L_b = d(N_b + 1), \quad N_b = \left(\frac{L_0}{d}\right) - 2C + 1 \tag{5}$$

where L_b is the length of the body of the extension spring excluding the hooks, and N_b is the number of body coils. The wire diameter d can be computed from the decision variable C and the known outer diameter OD as $d = OD/(1 + C)$, and the mean coil diameter is $D = Cd$.

We can formulate a single-objective optimisation problem that maximises any one of the following factors of safety, defined as:

$$n_A = \frac{S_y}{(\sigma_A)_{max}}, \quad n_B = \frac{S_{sy}}{(\tau_B)_{max}}, \quad n = \frac{S_{sy}}{(\tau_{coil})_{max}} \tag{6}$$

The values of S_y and S_{sy} are obtainable from Table 2, and the specific values for $(\sigma_A)_{max}$, $(\tau_B)_{max}$, and $(\tau_{coil})_{max}$ shall be obtained by replacing F with F_{max}: the tensile load at maximum deflection y_{max} in Eqs. 2, 3, and 4. It should be noted that more importance must be given to the factor of safety n for the coil, as the hook radii r_1 and r_2, which influence n_A and n_B, can be adjusted independently. The single-objective optimisation can thus be defined as:

$$\begin{aligned} &\text{minimise } \frac{1}{n(C, r_2)} \\ &\text{subject to } L_0 = L_b + 2(r_1 + r_2) \\ &\qquad C \in [4, 12], \quad r_2 \in [0.5, 12] \end{aligned} \tag{7}$$

The force at maximum elongation F_{max} is computed using the following procedure:

$$F_{max} = F_i + k y_{max} \tag{8}$$

where F_i is the initial preload and k is the spring stiffness constant. The preferred range for initial torsional stress, induced by the initial preload, is determined by the following expression:

$$\tau_i = \left[\frac{33500}{\exp(0.105C)} \pm 1000\left(4 - \frac{C-3}{6.5}\right)\right]\frac{6.89}{1000}\ \text{MPa} \tag{9}$$

We shall choose the lower limit of τ_i from Eq. 9 as $(\tau_i)_{min}$ (for a higher factor of safety) to determine the minimum initial preload as:

$$F_i = \frac{(\tau_i)_{min}\pi d^3}{8D} \tag{10}$$

Now, the stiffness of the spring is determined as:

$$k = \frac{d^4 G}{8D^3 N_a}, \quad N_a = N_b + \frac{G}{E} \tag{11}$$

where N_a is the number of active coils. Substituting k and F_i into Eq. 8 yields F_{max}, which can then be back-substituted into Eq. 2 to obtain $(\sigma_A)_{max}$. Once $(\sigma_A)_{max}$ is determined, the factors of safety can be computed from Eq. 6.

2.6 Numerical example

The decision variables that minimise $1/n(C, r_2)$ (or maximise $n(C, r_2)$) are found to be $C = 12$ and $r_1 = 5.7692$ mm. The same set of decision variables were also found to maxmise the other two factor of safetys n_A and n_B. The remaining dependent variables are thus obtained as:

1. Wire diameter $d = OD/(1 + C) = 1.1538$ mm.
2. Mean coil diameter $D = Cd = 13.8462$ mm.
3. Hook radius $r_1 = 0.5D = 6.9231$ mm.
4. Number of body coils from Eq. 5: $N_b = 42$.
5. Number of active coils from Eq. 11: $N_a = 42.4085$.
6. Length of body coils from Eq. 5: $L_b = 49.6154$ mm.
7. Initial preload from Eq. 10: $F_i = 2.0674$ N.
8. Spring stiffness from Eq. 11: $k = 0.1608$ N/mm or 160.8 N/m.
9. Factors of safety: $n_A = 1.1709$, $n_B = 1.2534$, and $n = 1.3748$.

2.6.1 Wrench-feasible workspace (WFW)

The static equilibrium equations of the mechanism can be expressed in the following form:

$$\mathbf{A}_{2\times 3}\boldsymbol{t}_{c_{3\times 1}} = \boldsymbol{w}_{3\times 1} \tag{12}$$

where $\mathbf{A}$ is called the structure matrix, $\boldsymbol{t}_c = [T_{c1}, T_{c2}, T_{c3}]$ is the vector of cable actuation forces, $\boldsymbol{w}$ is the vector of external wrenches acting on the moving platform. A pose is wrench-feasible if, for a specific external wrench $\boldsymbol{w}$, there exist a vector of cable-actuation force such that [5]:

$$\boldsymbol{t}_{c_{min}} \leq \boldsymbol{t}_c = \mathbf{A}^{\dagger}\boldsymbol{w} + \boldsymbol{h}\lambda \leq \boldsymbol{t}_{c_{max}},\ \mathbf{A}^{\dagger} = \mathbf{A}^T(\mathbf{A}\mathbf{A}^T)^{-1} \tag{13}$$

where $\boldsymbol{t}_{c_{min}}$ (resp. $\boldsymbol{t}_{c_{max}}$) is the vector $\boldsymbol{t}_c$ when atleast one of the $T_{ci} = T_{c_{min}}$(resp. $T_{c_{max}}$), $i = 1, 2, 3$. $\boldsymbol{h}$ is the null-space of the structure matrix $\mathbf{A}$ and λ is a scalar multiplier.

2.6.2 Wrench feasible workspace for stockier proportions

For a square grid of $\theta, \psi \in [-40°,\ 40°]$, the WFW of the mechanism of slender proportions is presented in Fig. 3.

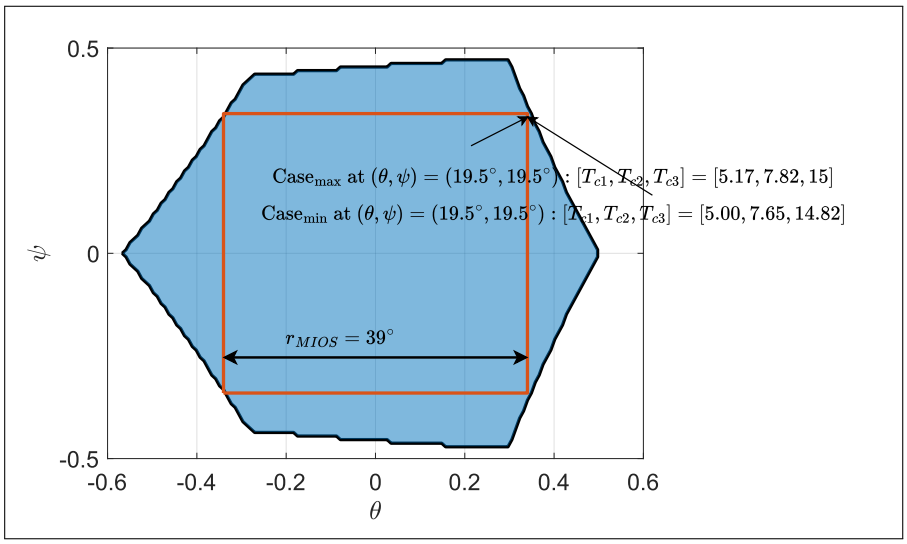

Figure 3: The WFW of the mechanism with stockier proportions. The origin-centered square that maximally inscribes the WFW has length of its side at 39°. Two cases of actuation forces at the common boundary of WFW and MIOS, at $(\theta, \psi) = (19.5°,\ 19.5°)$ are labelled. The spring designed as per the design strategy 1 has a spring index of $k = 160.8$ N/m.

The minimum and maximum cable-actuation forces are limited to the bounds $[T_{c_{min}},\ T_{c_{max}}] = [5\text{ N},\ 15\text{ N}]$. A maximally inscribing origin-centered square (MIOS) within the WFW boundaries, which can be used as a performance metric, has a side length of $r_{MIOS} = 39°$.

Two cases of cable-actuation forces at $(\theta, \psi) = (19.5°,\ 19.5°)$, a point at the common boundary of the WFW and MIOS, are also depicted in Fig. 3. Case$_{max}$ (resp. Case$_{min}$) corresponds to the condition when at least one of the actuation forces is at $T_{c_{max}}$ (resp. $T_{c_{min}}$). It should be noted from Case$_{max}$ that, at the boundary point $(\theta, \psi) = (19.5°,\ 19.5°)$, when T_{c3} was fixed at $T_{c_{max}}$, T_{c1} is very close to $T_{c_{min}}$. Similarly, in Case$_{min}$, when T_{c1} was fixed at $T_{c_{min}}$, T_{c3} is very close to $T_{c_{max}}$. A similar inference was made in [6] that, at the WFW boundaries, two of the three actuation forces will be at $T_{c_{min}}$ and $T_{c_{max}}$, respectively, while the third will take up a magnitude to maintain static equilibrium as per Eq. 12.

2.6.3 Wrench feasible workspace for slender proportions

For a mechanism with slender proportions, the entire square grid $\theta, \psi \in [-40°,\ 40°]$ is wrench feasible, as presented in Fig. 4. As before, the minimum and maximum cable forces are limited to the bounds $[T_{c_{min}},\ T_{c_{max}}] = [5\text{ N},\ 15\text{ N}]$. Two instances of actuation forces, Case$_{max}$ and Case$_{min}$, are labelled in Fig. 4. In Case$_{max}$, T_{c3} is fixed at $T_{c_{max}}$. However, neither of the other two forces, T_{c1} nor T_{c2}, is close to $T_{c_{min}}$, indicating that the true boundary of the WFW lies beyond the point $(\theta, \psi) = (40°,\ 40°)$. In Case$_{min}$, $T_{c1} = T_{c_{min}}$, and neither of the remaining two actuation forces, T_{c2} and T_{c3}, are close to $T_{c_{max}}$, which points to the same conclusion as above: the true WFW boundary lies beyond the point $(\theta, \psi) = (40°,\ 40°)$.

3 Design strategy 2: Spring constant considered as an additional input

Here, a new spring is designed for the 2-RRS-1-RRRR mechanism of various proportions. For any set of link proportions of the mechanism, the free length and maximum extended length can be determined based on specific configurations of the mechanism. In addition to the limits on free length and maximum extended length, the spring constant will also be considered as a design variable. A numerical example for the mechanism with slender proportions is presented below.

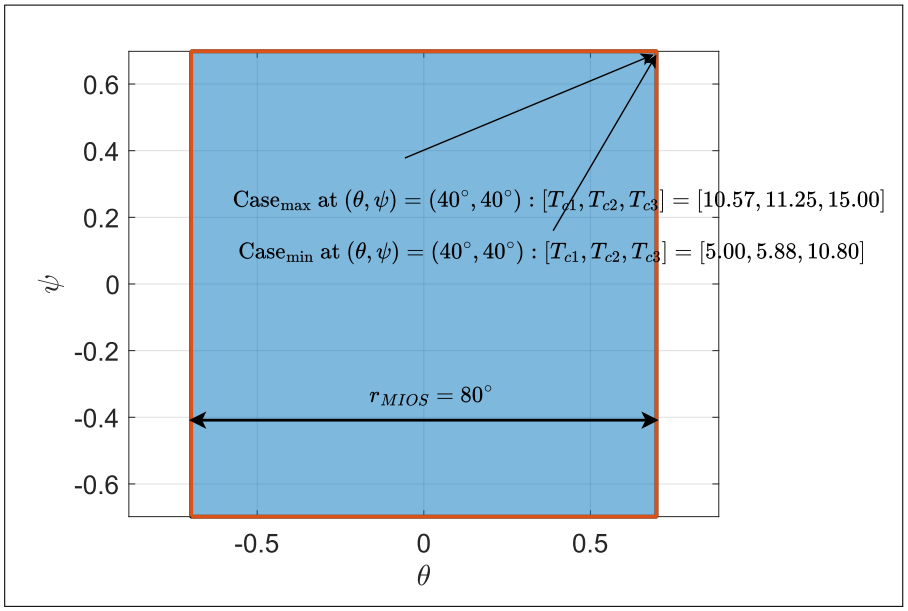

Figure 4: The WFW of the mechanism at slender proportions. The entire square grid $(\theta, \psi) \in [-40^\circ, 40^\circ]$ considered in this study is wrench feasible. Two instances of cable-actuation forces at the point $(\theta, \psi) = (40^\circ, 40^\circ)$ are labelled. The spring designed as per design strategy 1 has a spring constant of $k = 160.8$ N/m.

3.1 A numerical example of spring design for a mechanism with slender proportions

Here, a new spring is designed for various proportions of the 2-RRS-1-RRRR mechanism. For any set of link proportions of the mechanism, the limits for free length and maximum extended length can be determined based on specific configurations of the mechanism. In addition to the limits on free length and maximum extended length, a desired value of the spring constant will also be specified as a design requirement.

3.1.1 Design requirements

- The free length L_0 should be less than the minimum distance $L_{min} = 119.4135$ mm between the attachment points on the base and top platforms. L_{min} occurs at location 2 (resp. location 3), i.e., $(r', 210^\circ)$ (resp. $(r', 330^\circ)$) at $\theta, \psi = 40^\circ,\ -40^\circ$ (resp. $\theta, \psi = 40^\circ,\ 40^\circ$).

- The maximum extended length should be 10 mm greater than the maximum distance between the attachment points on the base and

top platforms. The maximum distance $L_{max} = 232.1899$ mm occurs at location 2 (resp. location 3) at $\theta, \psi = -40°, 40°$ (resp. $\theta, \psi = -40°, -40°$).

- The desired spring constant is 250 N/m.
- The spring index should lie between 4 and 12.
- The three factors of safety in Eq. 6 should preferably be within the limits of 1.25 and 1.35.
- The outer diameter is fixed at 15 mm for practical considerations.
- As before, the hook radius r_1 is taken as $D/2$.

3.2 Design procedure

- As before, the spring index $C \in [4,\ 12]$ and the hook radius $r_2 \in [1.75,\ 7.4]$ are considered the decision variables.
- The wire diameter d is evaluated as $d = \frac{OD}{C+1}$.
- The mean coil diameter D is evaluated as $D = Cd$.
- The number of active coils is evaluated as $N_a = \frac{d^4 G}{8D^3 k}$.
- The number of body coils is $N_b = N_a - \frac{G}{E}$.
- The free length is approximated as $L_0 \approx d(N_b + 1) + 2(r_1 + r_2)$.
- The maximum elongation from the free length is $y_{max} = L_{max} + 10 - L_0$.
- The prestress F_i for the spring is computed from Eq. 10.
- The load at maximum deflection is $F_{max} = F_i + k y_{max}$.
- The critical stresses and the factors of safety can then be calculated from Eqs. 2–4 and Eq. 6.

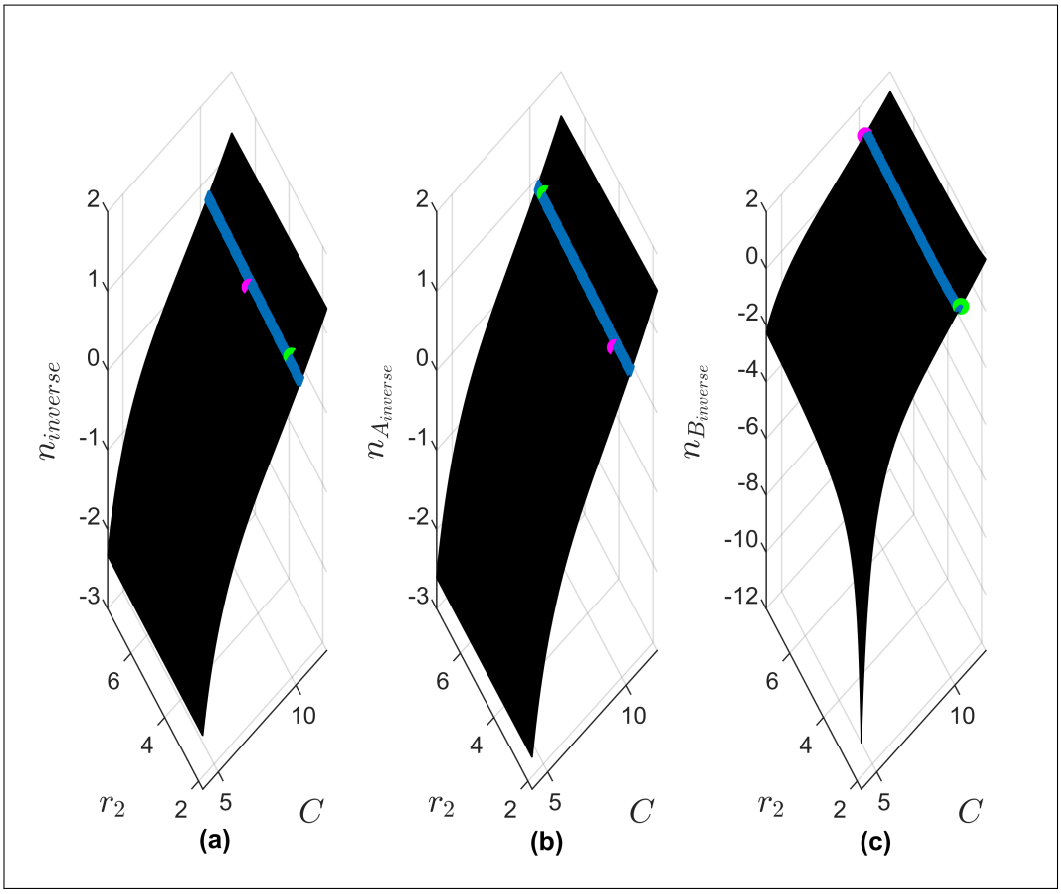

Figure 5: Variation of the inverse factors of safety $1/n$, $1/n_A$, and $1/n_B$ with C and r_2. The blue highlights correspond to the regions where $0.74 \leq 1/n \leq 0.8$.

3.2.1 Constraint 1: $0.74 \leq 1/n \leq 0.8$

The inverses of the factors of safety $1/n$, $1/n_A$, and $1/n_B$ are evaluated over a grid of $C \in [4,\ 12]$ and $r_2 \in [1.75,\ 7.4]$, and are presented in Fig. 5.

The highlighted region in Fig. 5a corresponds to the range $1/n \in [0.74,\ 0.8]$ (equivalently, $n \in [1.25,\ 1.35]$). The decision variables corresponding to this range are denoted as $(\boldsymbol{C^*},\ \boldsymbol{r_2^*})$. The ranges for $1/n_A$ and $1/n_B$ corresponding to $(\boldsymbol{C^*},\ \boldsymbol{r_2^*})$ are highlighted in Figs. 5b and 5c, respectively. The minimum (magenta) and maximum (green) values of the inverse factors of safety within $(\boldsymbol{C^*},\ \boldsymbol{r_2^*})$ are also plotted in their respective subfigures. The corresponding ranges of factors of safety n, n_A and n_B are shown as parallel plots in Fig. 6.

It can be inferred that if the constraint $1.25 \leq n \leq 1.35$ (or equivalently, $0.74 \leq 1/n \leq 0.8$) is enforced, the values of n_A remain below the preferred

range of [1.25, 1.35].

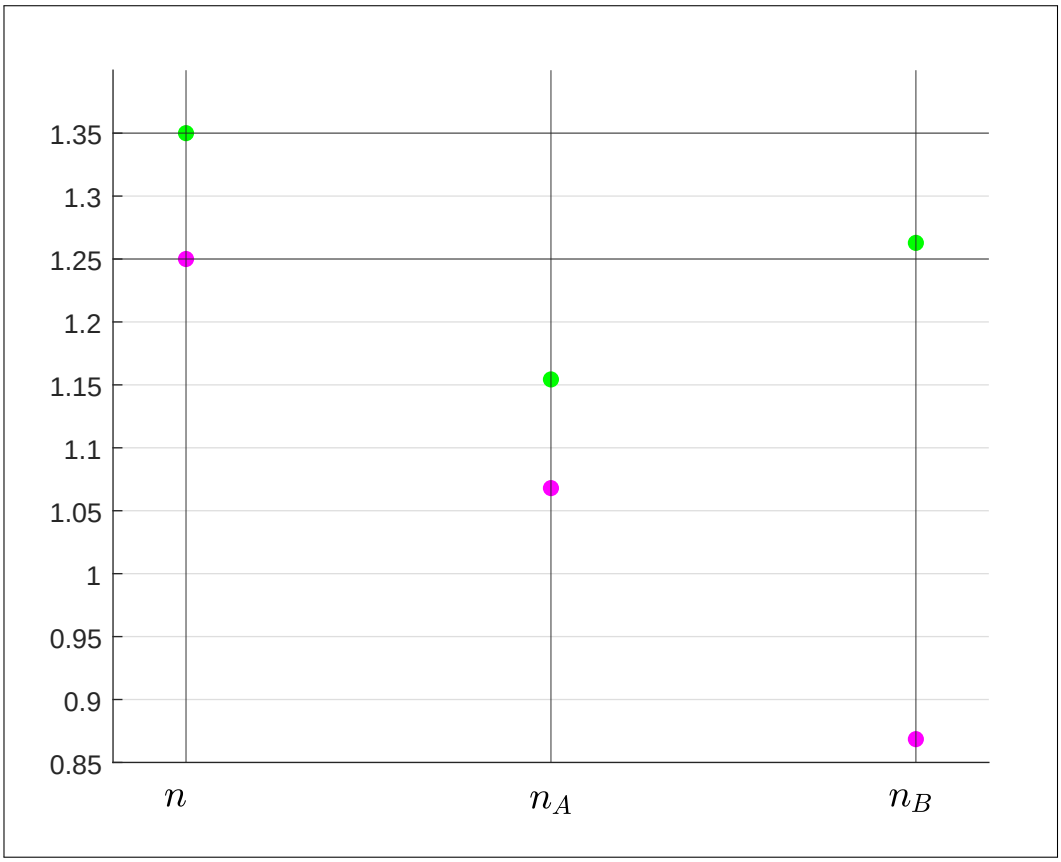

Figure 6: Parallel plot showing the ranges of n, n_A, and n_B corresponding to $(\boldsymbol{C^*},\ \boldsymbol{r_2^*})$.

3.2.2 Constraint 2: $0.74 \leq 1/n_A \leq 0.8$

Figure 7 presents the dependence of the inverse factors of safety $1/n_A$, $1/n$, and $1/n_B$, respectively, on C and r_2. The highlighted region in blue corresponds to the range $0.74 \leq 1/n_A \leq 0.8$. The corresponding set of decision variables shall be referred to as $\boldsymbol{(C^*, r_2^*)}$. The highlighted regions of $1/n$ in (b) and $1/n_B$ in (c) correspond to the decision variables $\boldsymbol{(C^*, r_2^*)}$. The minimum (magenta) and maximum (green) values of the inverse factor of safety within constraint 2 are also highlighted in Fig. 7. The minimum and maximum values of the factors of safety n_A, n, and n_B are presented as parallel plots in Fig. 8. It can be inferred that if constraint 2 is enforced, the range of n extends beyond the preferred limit of [1.25, 1.35], while the range of n_B fully encloses the preferred limit of [1.25, 1.35].

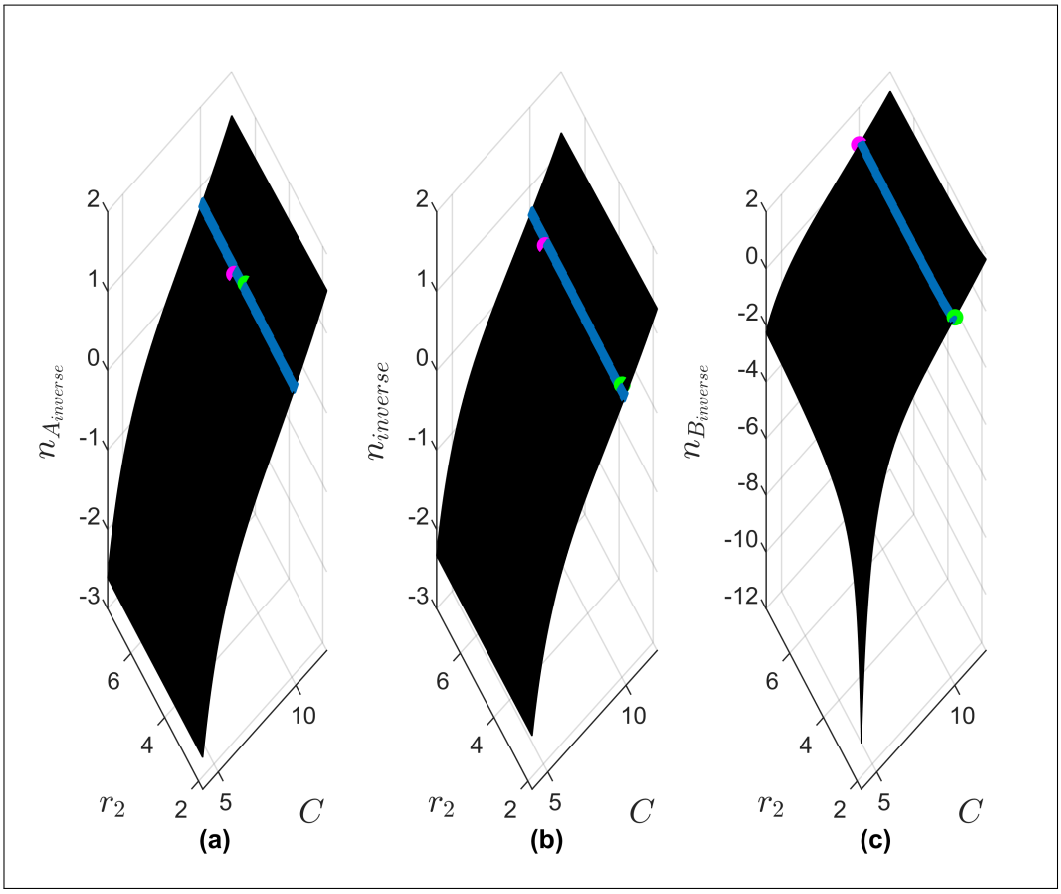

Figure 7: Variation of the inverse factors of safety $1/n$, $1/n_A$, and $1/n_B$ with C and r_2. The blue highlights correspond to the regions where $0.74 \leq 1/n_A \leq 0.8$.n

3.2.3 Constraint 3: $0.74 \leq 1/n_B \leq 0.8$

Here, the surface plots for the inverse factors of safety $1/n_B$, $1/n$, and $1/n_A$ are shown in Fig. 9. The blue-highlighted region in Fig. 9a corresponds to those that satisfy the constraint $0.74 \leq 1/n_B \leq 0.8$. The corresponding decision variables shall be referred to as $\boldsymbol{(C^*, r_2^*)}$. The highlighted regions of $1/n$ in Fig. 9b and $1/n_A$ in Fig. 9c correspond to the decision variables $\boldsymbol{(C^*, r_2^*)}$. The minimum (magenta) and maximum (green) values of the inverse factors of safety within $\boldsymbol{(C^*, r_2^*)}$ are also highlighted in Fig. 9. The minimum and maximum values of the factors of safety are presented as parallel plots in Fig. 10. It should be noted that if the constraint $1.25 \leq n_B \leq 1.35$ (or equivalently $0.74 \leq 1/n_B \leq 0.8$) is enforced, the minimum value of n lies within the preferred limits [1.25, 1.35], and the range of n_A fully encloses the

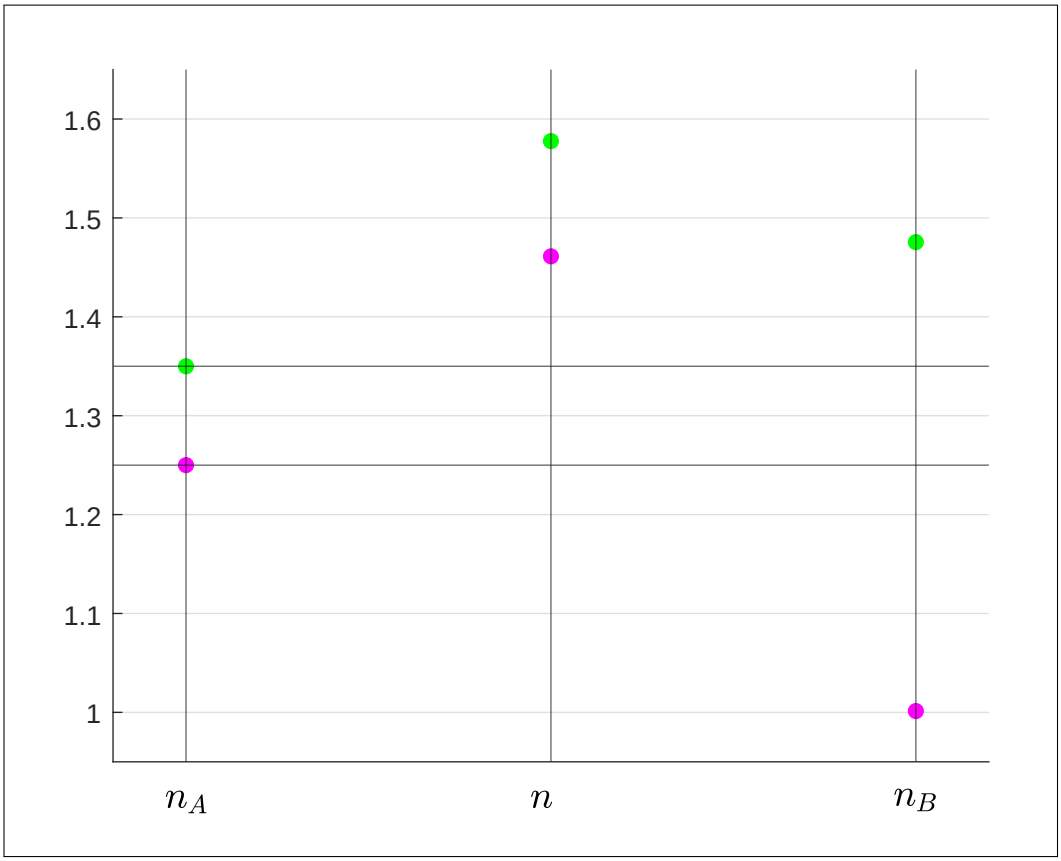

Figure 8: Parallel plot showing the ranges of n, n_A, and n_B corresponding to $(\boldsymbol{C}^*,\ \boldsymbol{r}_2^*)$.

preferred limits of [1.25, 1.35].

3.2.4 Formulating a constrained optimisation problem to find a suitable extension spring for a mechanism of slender proportions

Based on the inferences from Figs. 6, 8, and 10, the following constrained optimisation problems are formulated.

Problem 1

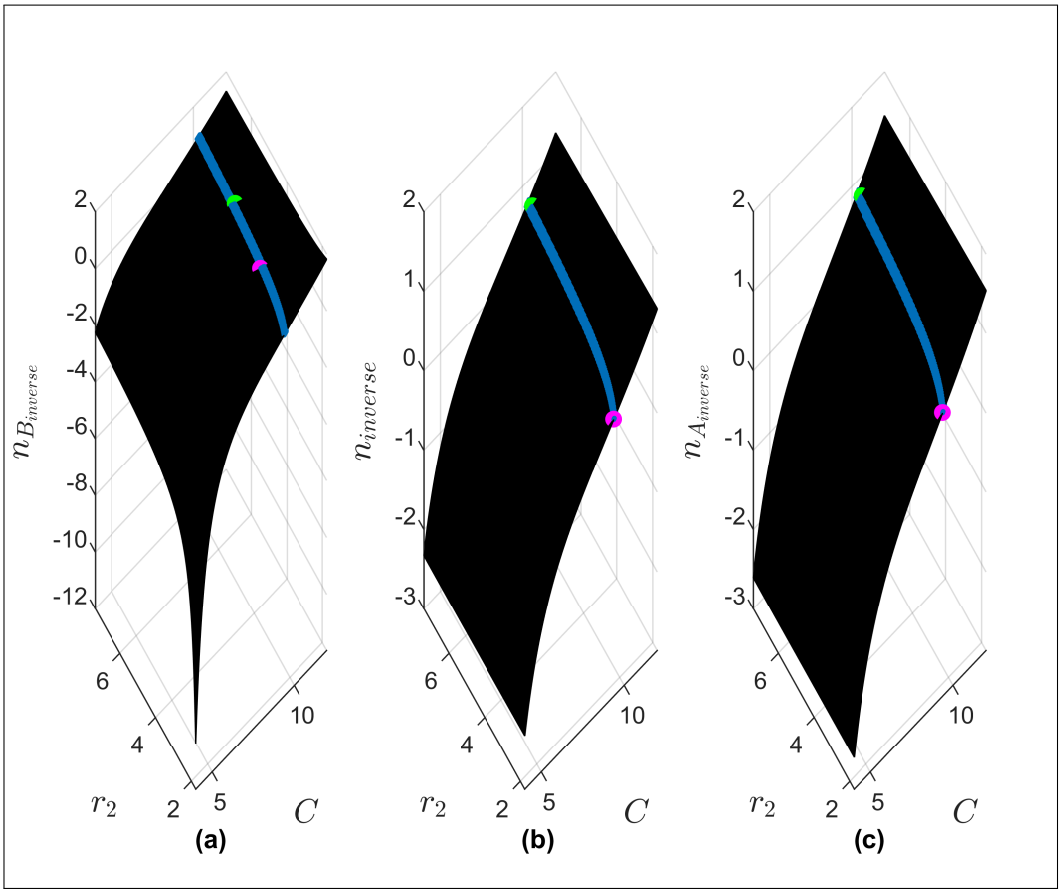

Figure 9: Variation of the inverse factors of safety $1/n$, $1/n_A$, and $1/n_B$ with C and r_2. The blue highlights correspond to the regions where $0.74 \leq 1/n_B \leq 0.8$.n

$$
\begin{aligned}
&\text{minimise } 1/n_A(C, r_2) \\
&\text{subject to } c_1 : d(N_b + 1) + 2(r_1 + r_2) - L_{min} < 0 \\
&\qquad\qquad c_2 : r_2 - r_1 < 0 \\
&\qquad\qquad c_3 : 1/1.35 - 1/n_A \leq 0 \\
&\qquad\qquad c_4 : 1/n_A - 1/1.25 \leq 0 \\
&\qquad\qquad c_5 : 1/1.35 - 1/n_B \leq 0 \\
&\qquad\qquad c_6 : 1/n_B - 1/1.25 \leq 0
\end{aligned}
\tag{14}
$$

Problem 2 is almost identical to Problem 1, except that the objective to be minimised is $1/n_B(C, r_2)$. The results of the above-defined constrained optimisation problems, along with the geometrical parameters of the spring

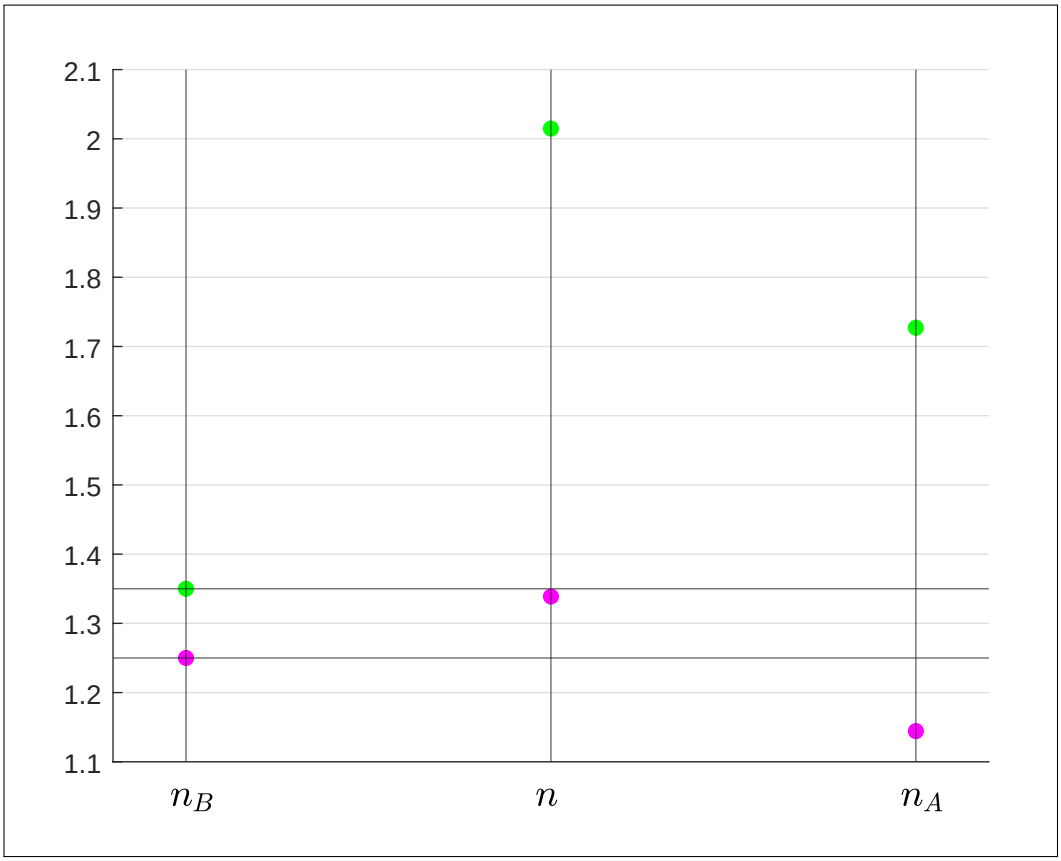

Figure 10: Parallel plot showing the ranges of n, n_A, and n_B corresponding to $(\boldsymbol{C}^*,\ \boldsymbol{r}_2^*)$.

corresponding to the optimal decision variables, are presented in Table. 3.

3.3 Numerical example of spring design for a mechanism with stockier proportions

This section repeats Section 3.1, except for small changes in the first two design requirements, which are stated as follows:

3.3.1 Design requirements

- The free length L_0 should be less than the minimum distance $L_{min} = 80.6628$ mm between the attachment points on the base and top platforms. L_{min} occurs at location 2 (resp. location 3) at radial coordinates $(r', 210°)$ (resp. $(r', 330°)$) for $(\theta, \psi) = (40°, -40°)$ (resp. $(\theta, \psi) = (40°, 40°)$).

	Problem 1	Problem 2
Optimal decision variables C, r_2	9.8814, 2.9500	9.9876, 4.2655
Free length L_0	100.7912	99.3895
Number of body coils N_b	57.9552	55.6699
Hook radius r_1	6.8108	6.8174
Mean coil diameter D	13.6215	13.6348
Wire diameter d	1.3785	1.3652
Initial tension F_i	4.6457	4.4497
Coil factor of safety n	1.5773	1.5289
Hook factor of safety against bending n_A	1.35	1.3082
Hook factor of safety against torsion n_B	1.2973	1.35

Table 3: Optimal decision variables and geometric parameters of of extension springs for the mechanism of slender proportions, obtained through the constrained optimisation problem.

- The maximum extended length should be 10 mm greater than the maximum distance between the attachment points on the base and top platforms. The maximum distance $L_{max} = 211.6892$ mm occurs at location 2 (resp. 3), having radial coordinates $(r', 210°)$ (resp. $(r', 330°)$) at $(\theta, \psi) = (-40°, 40°)$ (resp. $(\theta, \psi) = (-40°, -40°)$).
- The rest of the design requirements are similar to those presented in Sub-subsection 3.1.1. The design procedures formulated for the slender mechanism in Subsection 3.2 can be adopted for the stockier mechanism studied here.

Figure 11 presents the parallel plots for the three factors of safety when an extension spring is designed for a mechanism of stockier proportions. The bounds for the minimum and maximum values of the factors of safety presented in (a), (b), and (c) are obtained when the three constraints $(a)\ 0.74 \leq 1/n \leq 0.8,\ (b)\ 0.74 \leq 1/n_A \leq 0.8,\ (c)\ 0.74 \leq 1/n_B \leq 0.8$) are respectively enforced. It should be noted that the three parallel plots appear identical to the corresponding ones for the slender mechanism. Hence, we shall make use of the same constrained optimisation problem, formulated in Eq. 14, to find the feasible extension springs for a mechanism with stockier proportions.

3.3.2 Results of optimisation

Surprisingly, the results of the constrained optimisation did not converge! Until now, we were treating the spring constant k as an independent variable

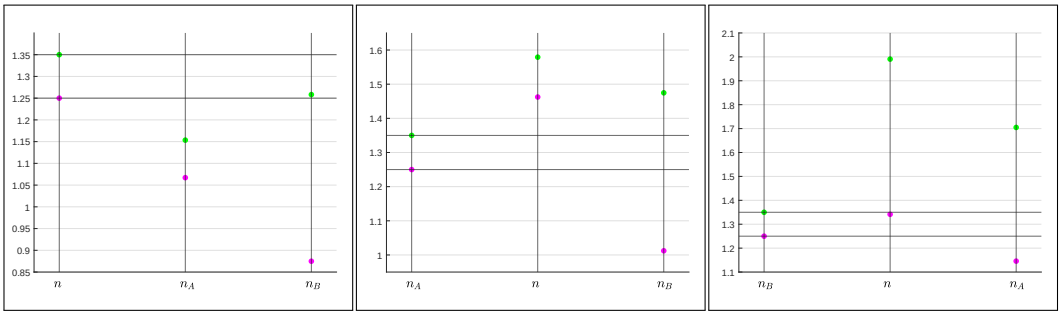

(a) (b) (c)

Figure 11: The bounds for the three factors of safety when the constraint $0.74 \leq 1/n \leq 0.8$ is enforced (Fig. 11a), when the constraint $0.74 \leq 1/n_A \leq 0.8$ is enforced (Fig. 11b) and when the constraint $0.74 \leq 1/n_B \leq 0.8$ is enforced (Fig. 11c).

and had not considered any realistic limits on the numerical values it could assume for a given design requirement. In the previous grid analysis on the factor of safety, the constraints were only on the preferred range of factors of safety. We had not considered whether the free length of the spring L_0 is lower than the minimum distance between the base and top platforms, L_{min}.

We have, however, considered this constraint on free length while performing a constrained optimisation (see c_1 in Eq. 14). By pure coincidence, the value of k considered at 250 N/m was compatible with all the constraints for the slender mechanism.

However, in the current case of the stockier mechanism, the requirement of $k = 250$ N/m makes the constraint $L_0 < L_{min}$ and the preferred range of factors of safety (1.25–1.35) incompatible. This can be explained through Fig. 12, which depicts the inverse factors of safety $1/n_B$, $1/n$, and $1/n_A$, respectively. The blue-highlighted region in Fig. 12a represents the values of $1/n_B$ lying in the preferred range $1/1.35 \leq 1/n_B \leq 1/1.25$. We shall refer to the corresponding decision variables as C^*, r_2^*. The inverse factors of safety $1/n$ and $1/n_A$ corresponding to C^*, r_2^* are highlighted in blue in Fig. 12b and c.

Furthermore, the inverse factors of safety corresponding to the decision variables C^{**}, r_2^{**} satisfying the free length constraint $L_0 < L_{min}$ (constraint c_1 in Eq. 14) are highlighted in yellow in all three plots. It should be noted that the blue and yellow regions do not intersect, indicating a constraint incompatibility. Thus, a feasible spring could not be designed with the current design requirements.

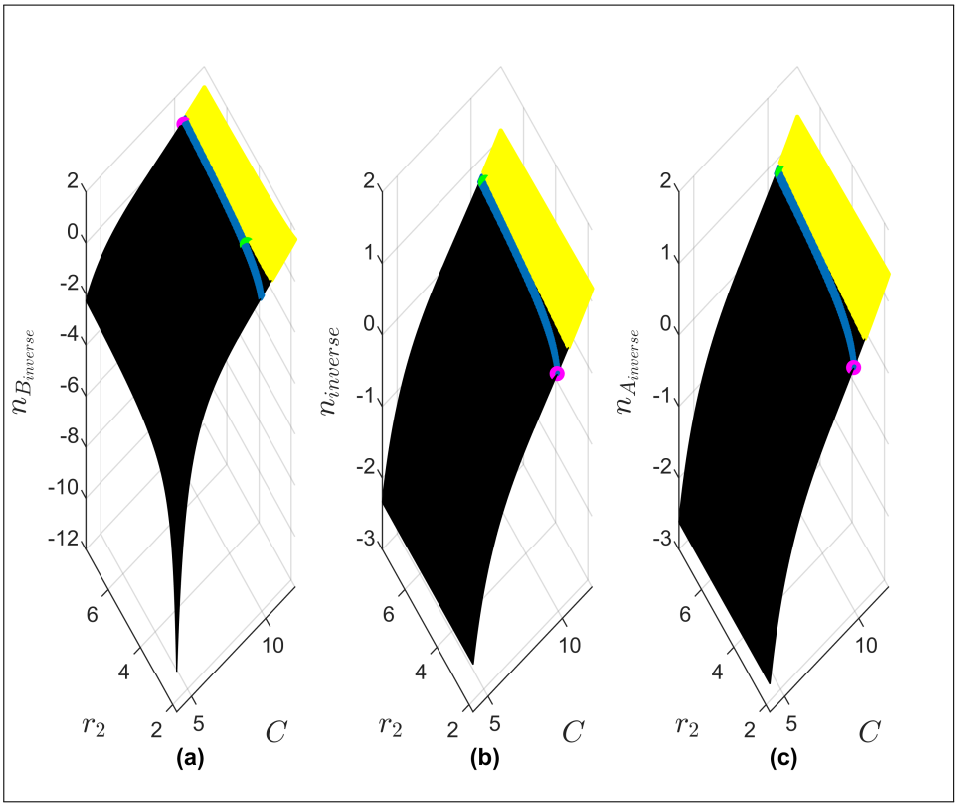

Figure 12: Variation of the inverse factors of safety $1/n_B$, $1/n$ and $1/n_A$ with the decision variables C and r_2. The blue highlights in each figure correspond to the regions satisfying the constraint $0.74 \leq 1/n_B \leq 0.8$. The yellow highlights depict the regions satisfying the free length constraint c_1 from Eq. 14.

3.3.3 Modifying the design requirement on spring constant

The above Fig. 12 is reproduced below as Fig. 13, with the spring constant k lowered from 250 N/m to 180 N/m. Unlike the previous case, the constraints imposed due to the preferred range of factor of safety (highlighted in blue) and the free length constraint L_0 (highlighted in yellow) are found to intersect, implying compatibility among constraints. The maximum and minimum values of all the factors of safety, satisfying all the constraints, are presented as parallel plots in Fig. 14.

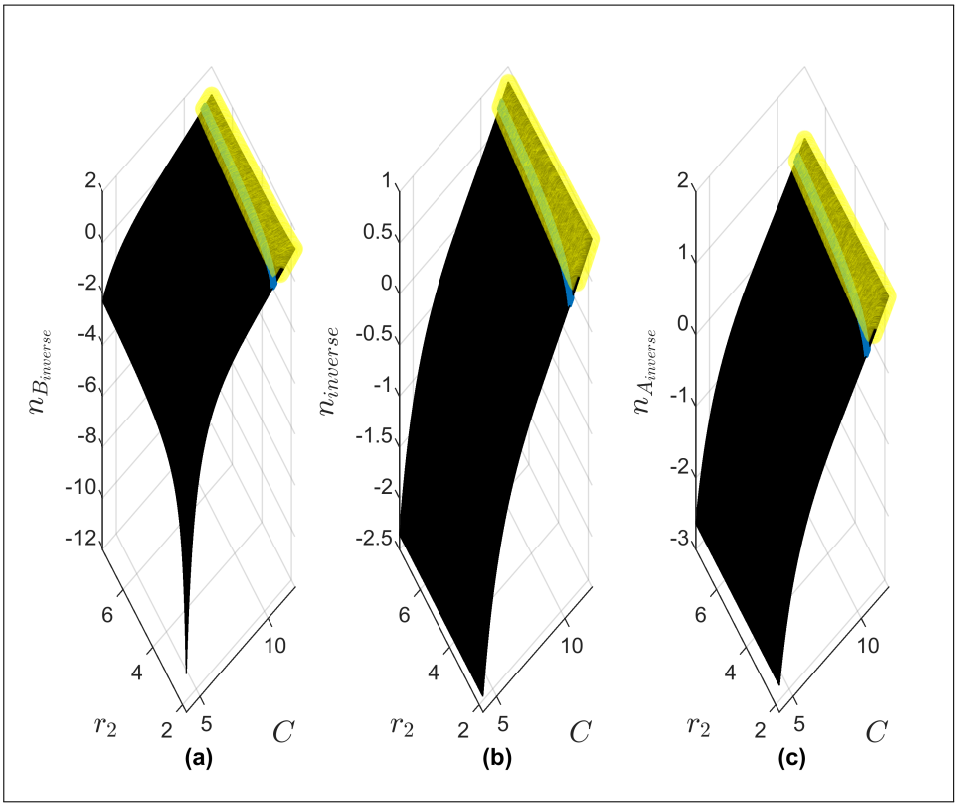

Figure 13: Variation of factors of safety with C and r_2. The blue highlights represent regions where the constraint $0.74 \leq 1/n_B \leq 0.8$ is valid. The yellow highlights represent the regions where the free length constraint c_1 from Eq. 14 is satisfied. The intersection of the two constraints implies constraint compatibility when the spring constant is lowered to 180 N/m.

3.3.4 Re-running the constrained optimisation with (reduced) $k = 180$ N/m for the mechanism with stockier proportions

The two constrained optimisation problems from Eq. 14 are executed once again, but with a lowered value of the spring constant at $k = 180$ N/m. The optimal decision variables and the geometrical parameters of the springs for the two problems are presented in Table 4.

3.4 Inferences from design strategy 2

Initially, the major requirements for designing an extension spring for a 2-RRS-1-RRRR mechanism were: 1) it should have a spring constant of 250 N/m, and 2) all three factors of safety should be in the range [1.25–1.35].

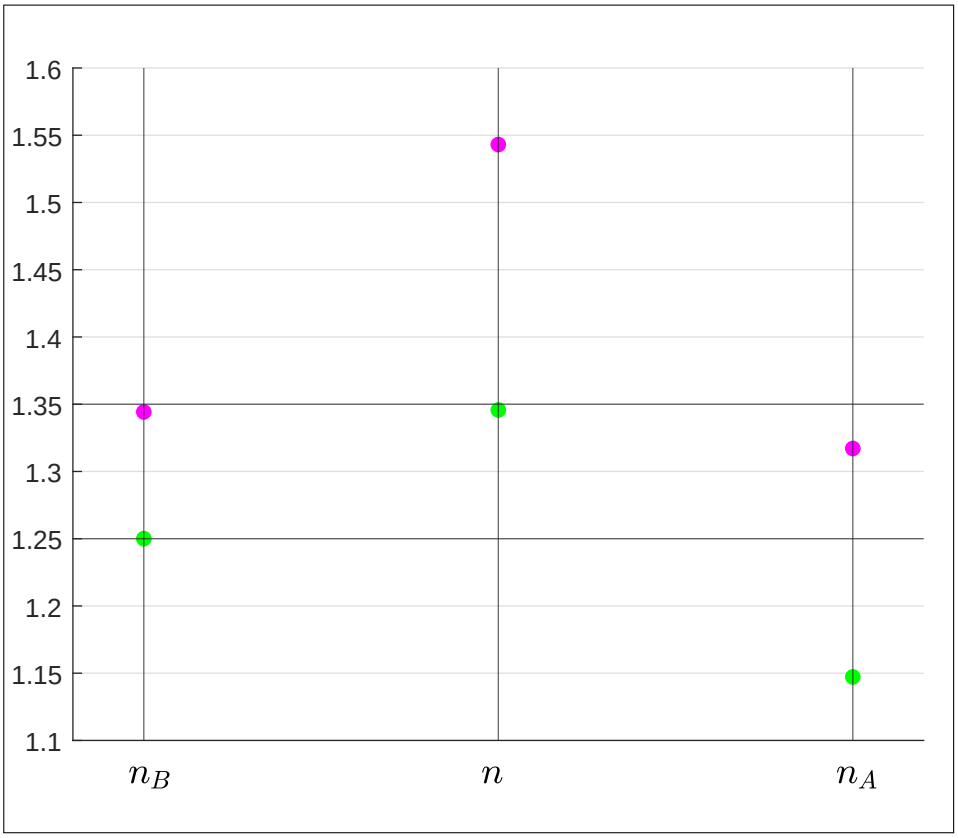

Figure 14: Parallel plots depicting the maximum and minimum values of the factors of safety n_B, n and n_A satisfying the constraint $0.74 \leq 1/n_B \leq 0.8$ and the free length constraint c_1 from Eq. 14, when the spring constant is lowered to 180 N/m.

Furthermore, the minimum distance between the base and top platforms should be greater than the free length of the spring, and the maximum distance between the base and top platforms should be less than the maximum extendable length of the spring. The two designs obtained for a mechanism of slender proportions (see Table 3) conformed to the above-mentioned constraints.

However, the spring designed for stockier proportions had constraint incompatibility between the free length constraint and the preferred range of factor of safety. By lowering the spring constant from 250 N/m to 180 N/m, the constraints were found to be compatible. With the lowered spring constant, the two designs thus obtained are presented in Table 4.

If it is desired to select a spring with a specific value of spring constant for various proportions of the 2-RRS-1-RRRR mechanism (say, for an opti-

	Problem 1	Problem 2
Optimal decision variables C, r_2	11.2749, 2.6774	11.4221, 4.1679
Free length L_0	78.9666	78.3580
Number of body coils N_b	47.9636	45.5661
Hook radius r_1	6.8890	6.8962
Mean coil diameter D	13.7780	13.7925
Wire diameter d	1.2220	1.2075
Initial tension F_i	2.6974	2.5534
Coil factor of safety n	1.5827	1.5323
Hook factor of safety against bending n_A	1.35	1.3066
Hook factor of safety against torsion n_B	1.2883	1.35

Table 4: Optimal decision variables and geometric parameters of extension springs for the mechanism of stockier proportions. The spring constant is $k = 180$ N/m.

mal design study of the mechanism), an appropriate spring constant must be selected through trial-and-error execution of the design strategy until the free length constraint (imposed by the stockier and slender proportions) and the preferred factor of safety constraint are compatible. Such a spring constant should be compatible for all mechanism proportions lying between the limiting cases of stockier and slender proportions.

For completeness of this study, the constrained optimisation problem is executed once again for the earlier case of the mechanism with slender proportions, but this time with a spring constant of 180 N/m. The results of the two design problems are presented in Table 5.

3.5 Wrench feasible workspaces

3.5.1 Stockier proportions

The WFW of the mechanism with stockier proportions is presented in Fig. 15. The minimum and maximum values of the actuation forces are bounded by $[T_{c_{min}},\ T_{c_{max}}] = [5\text{ N},\ 15\text{ N}]$. The maximally inscribed origin-centred square (MIOS) within the WFW has a length for its side of 34°. Two instances of actuation forces that maintain static equilibrium at the common boundary of the WFW and MIOS at $(\theta, \psi) = (17°,\ 17°)$ are labelled as Case_{max} and Case_{min} in Fig. 15.

In Case_{max}, T_{c3} is maintained at $T_{c_{max}}$ while T_{c1} is very close to $T_{c_{min}}$. Similarly, in Case_{min}, T_{c1} is maintained at $T_{c_{min}}$ and T_{c3} is very close to $T_{c_{max}}$.

	Problem 1	Problem 2
Optimal decision variables C, r_2	10.9386, 2.8007	11.0601, 4.1122
Free length L_0	88.5187	87.5892
Number of body coils N_b	54.0558	51.7947
Hook radius r_1	6.8718	6.8781
Mean coil diameter D	13.7436	13.7562
Wire diameter d	1.2564	1.2438
Initial tension F_i	3.0629	2.9246
Coil factor of safety n	1.5815	1.5355
Hook factor of safety against bending n_A	1.35	1.3104
Hook factor of safety against torsion n_B	1.2970	1.35

Table 5: Optimal decision variables and geometric parameters of extension springs of the mechanism with slender proportions. The spring constant is $k = 180$ N/m.

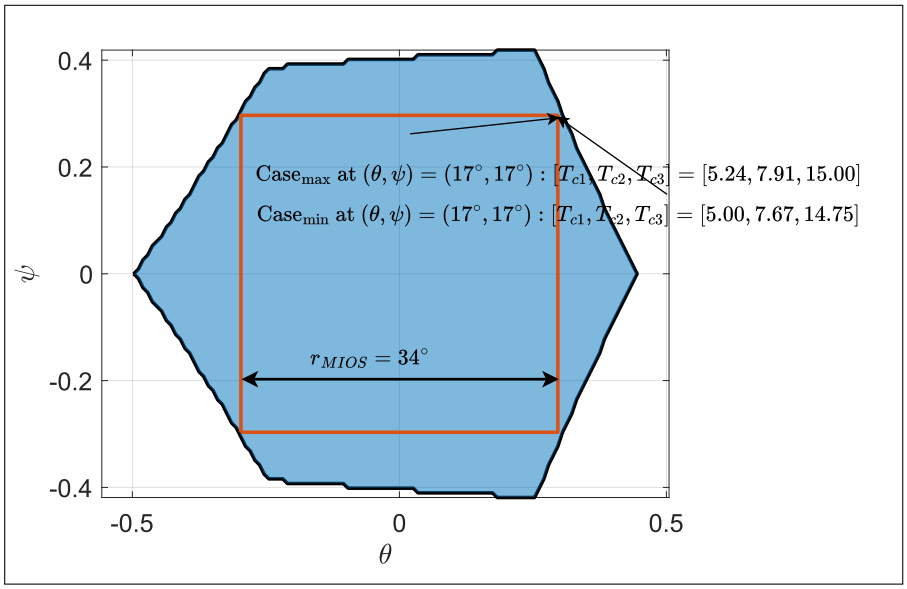

Figure 15: The WFW of the mechanism with stockier proportions. The origin centred square that maximally inscribes the WFW boundaries has the length of its sides at 34°. Two cases of actuation forces at the common boundaries of WFW and the maximally inscribed origin centred square (MIOS) at $(\theta, \psi) = (17^\circ,\ 17^\circ)$ are labelled. The spring design as per the design strategy two has a spring index of $k = 180$ N/m.

The corresponding forces in Case_{max} and Case_{min} being nearly equal, and two of the three forces in either case being close to $T_{c_{min}}$ and $T_{c_{max}}$, indicate

that the point $(\theta, \psi) = (17°,\ 17°)$ is very close to the true WFW boundary.

The spring used for the stockier mechanism has a spring constant of 180 N/m, and the rest of the geometrical parameters are as presented in Problem 1 of Table. 4.

3.5.2 Slender proportions

For a mechanism with slender properties, the entire square grid $\theta, \psi \in [-40°,\ 40°]$ is wrench-feasible as presented in Fig. 16. As before, the mini-

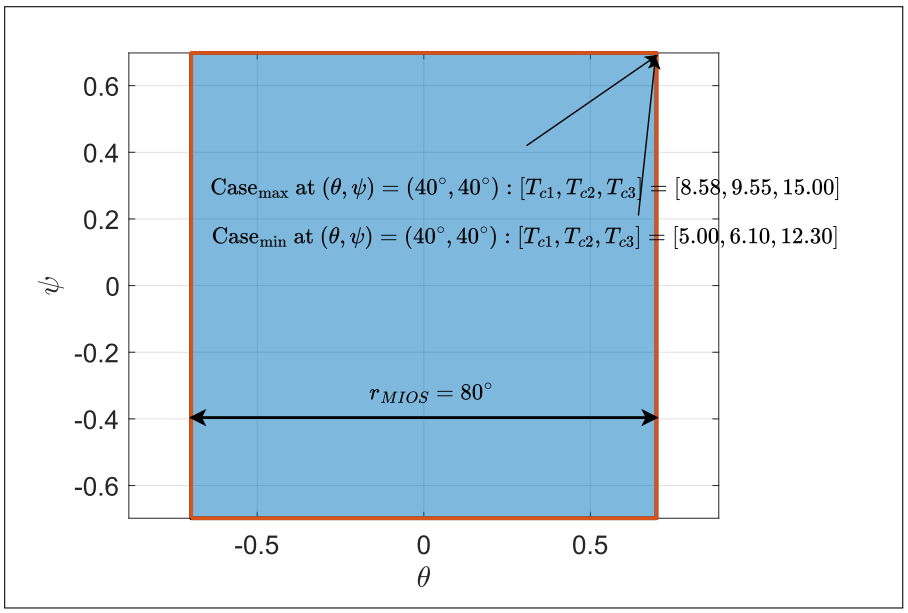

Figure 16: The WFW of the mechanism at slender proportions. The entire square grid $(\theta, \psi) \in [-40°,\ 40°]$ considered in this study is wrench feasible. Two instances of cable-actuation forces at one of the extreme point of the WFW at $(\theta, \psi) = (40°,\ 40°)$ is labelled. The spring design as per the design strategy 2 has a spring index of $k = 180$ N/m.

mum and maximum cable forces are limited to the bounds $[T_{c_{min}},\ T_{c_{max}}] = [5\text{ N},\ 15\text{ N}]$. Two instances of actuation forces, Case_{max} and Case_{min}, are labelled in Fig. 16. In Case_{max}, T_{c3} is fixed as $T_{c_{max}}$. However, none of the other two forces T_{c1} or T_{c2} are close to $T_{c_{min}}$, indicating that the true boundary of the WFW is beyond the point $(\theta, \psi) = (40°,\ 40°)$. In Case_{min}, $T_{c1} = T_{c_{min}}$, and the remaining two actuation forces T_{c2} and T_{c3} are not close to $T_{c_{max}}$, which points to the same conclusion as above: that the true WFW boundary is beyond the point $(\theta, \psi) = (40°,\ 40°)$.

References

[1] Isaac John, Santhakumar Mohan, and Philippe Wenger. Inverse kinematics of the 2-rrs-1-rrrr cable actuated mechanism, 2025. EngrXiv preprint, submitted to the 8th International Workshop on Computational Kinematics (CK2025).

[2] Isaac John, Santhakumar Mohan, and Philippe Wenger. Kinetostatic analysis of a spatial cable-actuated variable stiffness joint. *Journal of Mechanisms and Robotics*, 16(9):091003, 02 2024.

[3] J Keith Nisbett and Richard G Budynas. *Shigley's mechanical engineering design*. McGraw-Hill New York, 2011.

[4] P. S. Tan, Ali Akhavan Farid, Atefeh Karimzadeh, Seyed Saeid Rahimian Koloor, and Michal Petrů. Investigation on the curvature correction factor of extension spring. *Materials*, 13(18), 2020.

[5] Andreas Pott and Tobias Bruckmann. *Cable-driven parallel robots*, volume 116. Springer, 2013.

[6] Karol Muñoz, Mathieu Porez, and Philippe Wenger. Modeling and analysis of a four-leg tensegrity mechanism. *Mechanism and Machine Theory*, 211:106009, 2025.